Femtosecond covariance spectroscopy

Jonathan Owen Tollerud[a,b,1], Giorgia Sparapassi[a,b,1], Angela Montanaro[a,b], Shahaf Asban[c], Filippo Glerean[a,b], Francesca Giusti[a,b], Alexandre Marciniak[a,b], George Kourousias[b], Fulvio Billè[b], Federico Cilento[b], Shaul Mukamel[c,2], and Daniele Fausti[a,b,d,2]

[a]Physics Department, University of Trieste, 34127 Trieste, Italy; [b]Elettra-Sincrotrone Trieste S.C.p.A., 34149 Trieste, Italy; [c]Chemistry Department, University of California, Irvine, CA 92617; and [d]Department of Chemistry, Princeton University, Princeton, NJ 08544

Contributed by Shaul Mukamel, January 23, 2019 (sent for review December 12, 2018; reviewed by Peter Hamm and Alfred Leitenstorfer)

The success of nonlinear optics relies largely on pulse-to-pulse consistency. In contrast, covariance-based techniques used in photoionization electron spectroscopy and mass spectrometry have shown that a wealth of information can be extracted from noise that is lost when averaging multiple measurements. Here, we apply covariance-based detection to nonlinear optical spectroscopy, and show that noise in a femtosecond laser is not necessarily a liability to be mitigated, but can act as a unique and powerful asset. As a proof of principle we apply this approach to the process of stimulated Raman scattering in α-quartz. Our results demonstrate how nonlinear processes in the sample can encode correlations between the spectral components of ultrashort pulses with uncorrelated stochastic fluctuations. This in turn provides richer information compared with the standard nonlinear optics techniques that are based on averages over many repetitions with well-behaved laser pulses. These proof-of-principle results suggest that covariance-based nonlinear spectroscopy will improve the applicability of fs nonlinear spectroscopy in wavelength ranges where stable, transform-limited pulses are not available, such as X-ray free-electron lasers which naturally have spectrally noisy pulses ideally suited for this approach.

impulsive stimulated scattering | ultrafast spectroscopy | stochastic light

Noise, intrinsic to the measurement of any physical quantity, is normally seen as a limitation to eliminate. The desired signal-to-noise ratio is commonly reached by (*i*) mitigating as much as possible the amount of experimental noise and (*ii*) taking the mean of a large number of repeated "identical" measurements. From an alternative perspective, where every repetition is considered to be a measurement under different conditions, noise can become an asset and be exploited as a source of additional information (1–4). In this case, since the measurements are performed under different conditions, the mean value loses significance and other statistical tools such as higher-order moments are needed. If treated properly, noise can help clarify the interpretation of experiments (5) and even amplify signals as in stochastic resonance schemes (6).

Femtosecond nonlinear optical spectroscopy is ideally suited for an approach based on high-order moments. In standard mean-value nonlinear spectroscopies, the nonlinear signals are often extremely weak relative to the linear ones and complicated experimental layouts are required to separate them. Pulsed sources typically have several amplification stages, which naturally lead to significant noise in the output, further complicating the detection (7). To deal with these challenges, significant effort and investment has gone into engineering stable laser sources, and the stability requirements have influenced experimental design and technique development (8–10). Laser cost and experimental complexity have limited the adoption of many extremely useful but overly difficult techniques [such as multidimensional spectroscopy, fs-stimulated Raman scattering (fs-SRS), etc.].

Pioneering works by Lau and Kummrow (11, 12) in the 1980s and 1990s and more recently by Turner et al. (13) have shown that temporally incoherent (up to ns) pulses can be used in place of transform limited fs pulses to perform various nonlinear spectroscopic studies (14, 15) including coherent anti-Stokes Raman spectroscopy and 2D electronic spectroscopy without compromising on the required fs time resolution. These approaches are different from the present study since they require each set of pulses to be identical copies, and use traditional multibeam geometries and mean-value detection.

We can instead consider each laser pulse in a femtosecond nonlinear experiment as a measurement under different conditions rather than a repetition of the same experiment. The spectrum of a nonlinear signal in an *N*-wave mixing experiment depends on the product of the excitation fields (10, 16), and will thus change with the pulse-to-pulse fluctuations in the laser. In the approach proposed here we show that in the presence of spectrally narrow pulse-to-pulse fluctuations, the nonlinear sample response imprints correlations between the spectral components within the laser bandwidth. After recording each unique optical signal, we use it to calculate the covariance between intensities at different frequencies, rather than averaging all of the signals out as in mean-value approaches. Evaluating the frequency difference between those spectral components whose covariance is different from zero, we retrieve the energy of the sample excited states that have interacted with the radiation and thus introduced the optical correlation. From this viewpoint, it is clear that the larger are the

Significance

Here we establish femtosecond covariance spectroscopy as a technique that uses ultrashort stochastic light pulses to measure nonlinear material responses. By using pulses with spectrally uncorrelated fluctuations we can leverage on the noise and consider each repetition of the experiment as a measurement under different conditions. In this limit we demonstrate that nonlinear processes in the sample can be retrieved by measuring the spectral correlations in different pulses. We validate the approach by studying stimulated Raman scattering in α-quartz. This concept can be applied to reveal low-energy modes of electronic, spin, and vibrational origin and adapted to different techniques and wavelength ranges, from optical to X-ray free-electron lasers, where strong stochastic fluctuations are unavoidable.

Author contributions: D.F. conceived and led the project; J.O.T., G.S., and A. Montanaro performed the experiment; F. Glerean, F. Giusti, A. Marciniak, F.C., and D.F. contributed to performing the experiments; G.S., A. Montanaro, G.K., and F.B. developed the necessary code for data analysis and performed it; S.A. and S.M. developed the theoretical model; and J.O.T., G.S., and D.F. wrote the paper with contributions from all the other authors.

Reviewers: P.H., University of Zurich; and A.L., University of Konstanz.

The authors declare no conflict of interest.

[1]J.O.T. and G.S. contributed equally to this work.

[2]To whom correspondence may be addressed. Email: smukamel@uci.edu or daniele.fausti@elettra.eu.

This article contains supporting information online at www.pnas.org/lookup/suppl/doi:10.1073/pnas.1821048116/-/DCSupplemental.

Published online February 28, 2019.

stochastic fluctuations in the optical pulse, the smaller are the correlations between the pulse components before the interaction, and the better the sample nonlinear response is explored. Thus, adding a spectrally uncorrelated (i.e., spectrally narrow) stochastic element to each excitation pulse is the key to improve the covariance-based approach. There has recently been some effort in combining single-pulse detection with metrics beyond mean value for detection of signals at the shot-noise level (17–19); however, so far there has been no demonstration of enhancement of uncorrelated noise at a classical level to improve detection of spectral correlations in a nonlinear experiment.

In this article, we use covariance-based measurements to study vibrational modes in a crystalline quartz sample via SRS. When repeated many times with different unique noise realizations, the amplitudes of the different spectral components within the pulse bandwidth that are separated by the sample phonon frequencies become correlated (see *SI Appendix, Model* for a microscopic description of the experiment). We stress that all of these correlated fluctuations are averaged out or never resolved in mean-value measurements, whereas the frequency-resolved covariance of the transmitted pulses contains valuable insight on the SRS processes, and the energies of the phonons involved. Importantly, the framework used here to reveal SRS could be generalized to other nonlinear optical techniques based both on tabletop and free-electron laser (FEL) sources (20). X-ray FELs pose a particularly attractive possibility because they function based on self-amplified spontaneous emission which intrinsically leads to noisy pulses optimally suited to covariance-based techniques.

Results

In the present demonstration of femtosecond covariance spectroscopy, ultrafast pulses from a regenerative amplifier (~40 fs) are transmitted through the sample and the spectrum of each transmitted pulse is detected using a spectrometer that consists of a grating and a fast photodiode array detector.

A stochastic element in the form of spectrally uncorrelated pulse-to-pulse noise can be added in several ways. We utilize a programmable liquid crystal spatial light modulator based pulse shaper (21) placed between the laser and the sample as sketched in Fig. 1*B*. The pulse shaper changes the spectral phase with a defined modulation amplitude and correlation length ($\pm\pi/2$ rms, 0.25 THz, respectively). A reference beam is routed around the sample to a second identical spectrometer so we can compare the spectral covariance with and without interacting with the sample.

The time profiles resulting from the application of a spectral phase to initially transform limited pulses can be divided into a short coherent component (blue spike in Fig. 1*A*) which provides the impulsive excitation of the Raman modes, and noisy incoherent tails which probe the mode. Over the course of many noise realizations the average of the noisy tails becomes a roughly 1-ps Gaussian pulse, shown in green in Fig. 1*A*.

In a typical measurement, we record sample and reference pulse spectra for 50,000 different noise realizations. We then use a covariance-based analysis to extract information about the sample through correlations induced by SRS. While more diverse covariance metrics could be used, we consider the Pearson coefficient, which quantifies the degree of linear correlation between two random variables, the measured intensity I at the frequencies ω_i and ω_j within the pulse bandwidth:

$$P\left(I(\omega_i), I(\omega_j)\right) = \left[\left\langle I(\omega_i) I(\omega_j)\right\rangle - \left\langle I(\omega_i)\right\rangle\left\langle I(\omega_j)\right\rangle\right] / \left(\sigma_i \sigma_j\right),$$

where the angular bracket indicates a mean across all measurements, and $\sigma_{i(j)}$ is the SD across all measurements of the intensity at frequency $\omega_{i(j)}$. $P = 1$ (-1) indicates perfect correlation (anti-correlation), while $P = 0$ indicates no correlation. The result of this data processing performed across all of the possible frequency combinations forms a 2D Pearson coefficient map, such as those shown in Fig. 1 *C* and *D*.

The P map calculated using the reference pulses, shown in Fig. 1*C*, exhibits no features apart from an area of positive correlation at $\omega_i = \omega_j$ (the diagonal of the map).

In contrast, when the pulse has interacted with the sample (Fig. 1*D*), the map is evidently structured. Most importantly, we observe signatures of correlation induced through SRS in the form of features offset of a quantity $\Delta\omega$ from the diagonal, with a finite width which depends on the linewidth of the resonance and the correlation length. By comparing the correlation map to the spontaneous Raman spectrum (22) (Fig. 1*E*), it is clear that $\Delta\omega$ matches the Raman shift of the main phonon features. The signal presence is substantiated by the fact that frequency components separated by Ω must have the same phase for interference between the paths leading to the population of that vibrational level to occur (23).

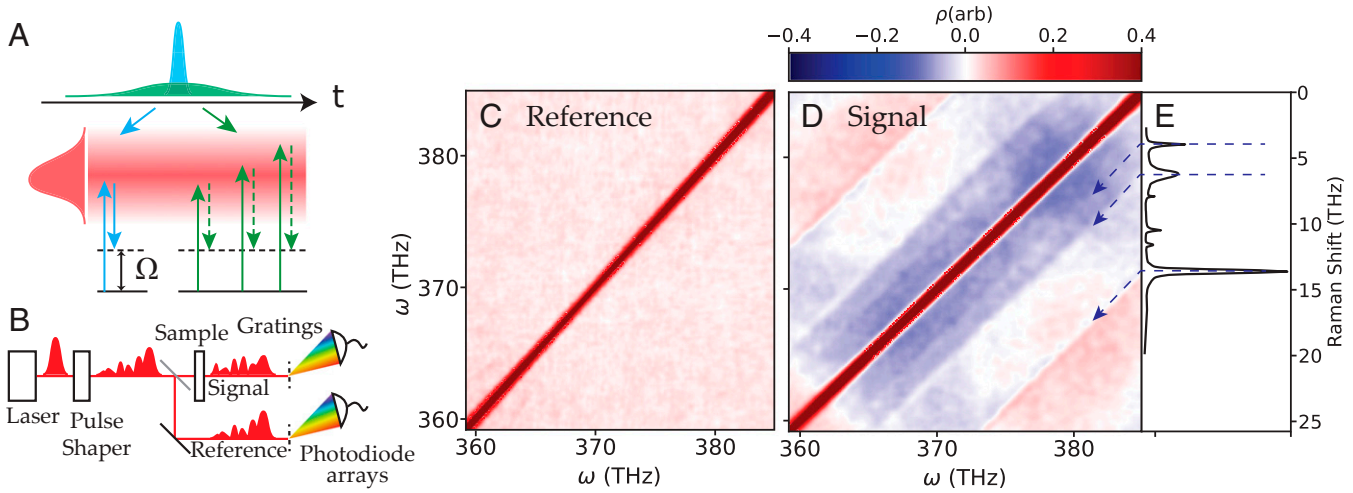

Fig. 1. (*A*) Simplified diagram of the SRS process, which induces correlations of spectral components at frequencies ω and $\omega \pm \Omega$. The shaped pulses can be divided into a coherent component (blue) and a noisy tail (green). (*B*) The experimental apparatus. (*C* and *D*) Pearson correlation plots for all pairs of frequencies within the excitation spectrum (*C*) after the pulse shaper, and (*D*) after the quartz sample. (*E*) Spontaneous Raman spectrum of quartz (14), matching the positions of the features in the covariance map in *D*.

To visualize the Raman shift of the SRS features as a function of Δω, the correlation data can be plotted as P (ω, Δω) instead of P (ω_i, ω_j) (there is a symmetric set of features for negative Δω which is left out of the plots in Fig. 2 for clarity purposes). Fig. 2*A* shows this for the same data as Fig. 1*D*. By taking the average Δω values of these maps along the ω-axis, we can better analyze the features. In Fig. 2*D*, we show the average for the three regions indicated in Fig. 2 *A*–*C*: this can be thought of as a sort of vibrational "spectrum," where the Raman features appear on top of a shifting background.

The programmable nature of the pulse shaper offers a broad flexibility in how the noise is introduced, which affects the visibility and the lineshape of the SRS features. Below, we explore two variations in which the noise is applied to only one-half of the spectrum (above $\omega_0 = 369$ THz). In the first variation (shown in Fig. 2*B*), the spectral amplitude of the noise-free half of the spectrum ($<\omega_0$) is shaped such that the average value of the excitation spectrum has a Gaussian profile. In the second example (shown in Fig. 2*C*), the spectral amplitude of the noise-free side is reduced to 0, so that the average excitation spectrum has a sharp edge at ω_0. In both cases, the features become more pronounced in the region quantifying the correlation between modulated and nonmodulated components, indicated by the black dashed boxes in Fig. 2 *A*–*C*. For comparison, the regions which quantify the correlation of two noisy frequencies have features similar to those achieved when the noise is applied uniformly across the entire spectrum.

The resonances we identify appear at the spontaneous Raman resonances of quartz (which are indicated by the gray dashed lines) (22). Clearly, the lineshape of these resonances depends on how the noise is applied. In most cases we observe a dispersive lineshape going from negative to positive values as Δω increases, except in the case of the red region in Fig. 2*C* which has purely positive peak shapes.

Discussion

The Raman process shifts spectral weight, which leads to spectral correlations that manifest as off-diagonal lines in the P maps. The mechanism underlying this shift in spectral weight could have several origins, some coherent or incoherent. An SRS process produces a four-wave mixing signal which is coherent and—when spectrally and spatially overlapped with the excitation pulse—leads to self-heterodyning of the excitation pulse and SRS signal. The results in Fig. 2 suggest that the process is coherent and stimulated; when there is a heterodyning field present at the emission energy (i.e., in Fig. 2 *A* and *B*) we observe dispersive peak shapes, but in the absence of a heterodyning field (Fig. 2*C*) we observe nondispersive peak shapes. This dependence of the peak shape on the presence of a heterodyning field confirms the sensitivity of our detection technique to the signal phase, and that the mechanism of the spectral weight shift is coherent, consistent with SRS.

The dispersive peak shapes can be understood by considering the effect of self-heterodyning on the spectrally resolved covariance. Regions where the signal and the excitation pulse are in phase should be positively correlated, as an increase in the excitation field will lead to a proportional increase in intensity at the signal frequency, due to constructive interference of the electric fields. Conversely, when signals and the pulse are out of phase, their correlation is negative as the interference will be destructive. The SRS signal has a π/2 phase shift relative to the excitation pulse due to the absorption and reemission processes, which is consistent with the observed dispersive shapes.

It is important to note that the correlation maps are fundamentally different from the more familiar intensity spectra. For example, multiple mechanisms may induce correlations for overlapping pairs of frequencies. The shape of the resulting features in a P map is the sum of all these mechanisms, taking into account the sign of the correlations, which could be mistaken for interference of electric fields.

We also note that P is not necessarily directly proportional to the amplitude of the nonlinear signal: a weak signal can be strongly correlated to other frequencies. While not intuitive, this feature also illustrates the power of covariance-based detection: weak signals in mean-value measurements are easily masked by noise, but can be detected in the covariance plots, even when the spectra fully spectrally and spatially overlap with the excitation pulse.

In this work, we have shown that covariance-based detection can be combined with noisy input pulses to resolve the SRS spectrum of a crystalline sample, and more incisive analytical tools than the average value can access a great depth of information that is missed by standard experiments. The transmitted pulses averaged over many noise realizations do not show the Raman resonances. However, the resonances are recovered in the covariance spectrum that reveals correlations between two spectral components separated by the phonon frequency. A high-resolution

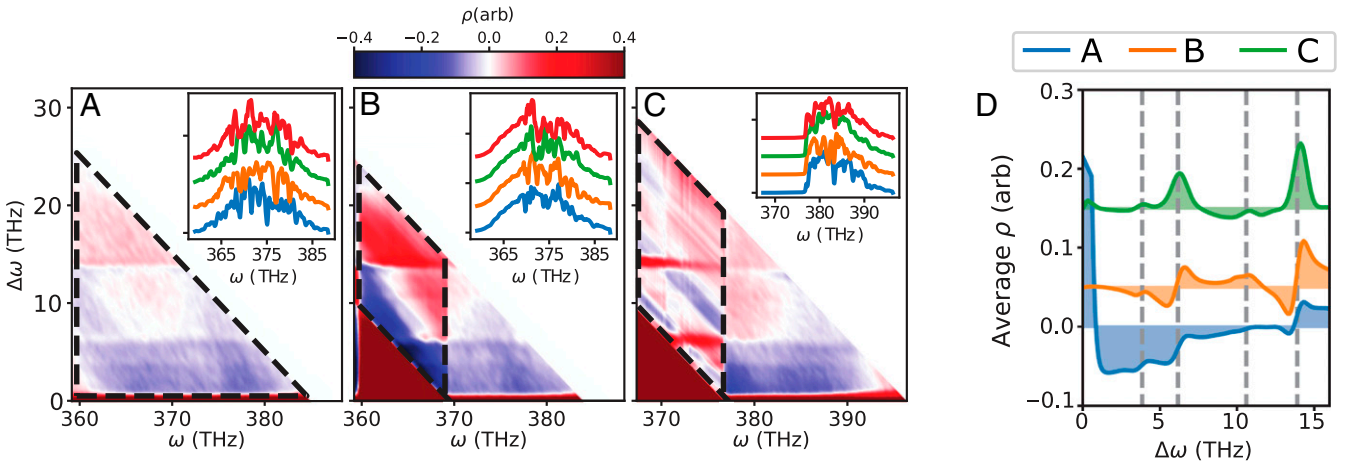

Fig. 2. Covariance maps recorded in α-quartz by applying uniform phase noise to each pulse. The noise is applied: (*A*) across the entire spectrum; (*B*) only to frequencies above 369 THz; and (*C*) as in *B*, but with mean-value shaping to eliminate the frequencies below 369 THz from the pulse spectrum. (*Insets*) Some detected pulse spectra. (*D*) SRS correlation spectra achieved by integrating the regions in *A*–*C* along the ω-axis indicated by the black dashed lines.

Raman spectrum is thus generated by exploiting the noise fluctuations, without the need for stable light sources.

We emphasize that this result is only one example of a broader class of covariance-based analysis tools that can be applied both using tabletop sources, where fluctuations can be controlled, as well as using SASE FELs where amplitude and phase noise are unavoidable (24).

Further, while the two frequency Pearson coefficient based framework demonstrates how correlations induced by nonlinear processes can be detected, we expect that other tailored statistical tools will reveal nonlinear processes at higher orders as done in multidimensional spectroscopy (25).

ACKNOWLEDGMENTS. This work was supported by the European Commission through the European Research Council (ERC) Starting Grant Inhomogenieties and Fluctuations in Quantum Coherent Matter Phases by Ultrafast Optical Tomography (INCEPT) (Grant 677488). S.M. gratefully acknowledges the support of the National Science Foundation (Grant CHE-1663822). S.M. and S.A. were supported by Chemical Sciences, Geosciences, and Biosciences Division, Office of Basic Energy Sciences, Office of Science, US Department of Energy Awards (DOE) DE-FG02-04ER15571 and DE-SC0019484.

1. Mikosch J, Patchkovskii S (2013) Coincidence and covariance data acquisition in photoelectron and -ion spectroscopy. I. Formal theory. *J Mod Opt* 60:1426–1451.
2. Frasinski LJ, Codling K, Hatherly PA (1989) Covariance mapping: A correlation method applied to multiphoton multiple ionization. *Science* 246:1029–1031.
3. Sigman ME, Williams MR (2006) Covariance mapping in the analysis of ignitable liquids by gas chromatography/mass spectrometry. *Anal Chem* 78:1713–1718.
4. Xu XG, Konorov SO, Hepburn JW, Milner V (2008) Noise autocorrelation spectroscopy with coherent Raman scattering. *Nat Phys* 4:125–129.
5. Kogan S (1996) *Electronic Noise and Fluctuations in Solids* (Cambridge Univ Press, Cambridge, UK).
6. Gammaitoni L, Hänggi P, Jung P, Marchesoni F (1998) Stochastic resonance. *Rev Mod Phys* 70:223–287.
7. Fausti D, van Loosdrecht PHM (2011) Time resolved Raman scattering. *Optical Techniques for Solid-State Materials Characterization*, eds Prasankumar RP, Taylor AJ (CRC Press, Boca Raton, FL).
8. Chen S, et al. (2014) Recovery of Raman spectra with low signal-to-noise ratio using Wiener estimation. *Opt Express* 22:12102–12114.
9. Bartels A, Hudert F, Janke C, Dekorsy T, Köhler K (2006) Femtosecond time-resolved optical pump-probe spectroscopy at kilohertz-scan-rates over nanosecond-time-delays without mechanical delay line. *Appl Phys Lett* 88:1–3.
10. Yan YX, Gamble EB, Jr, Nelson KA (1985) Impulsive stimulated scattering: General importance in femtosecond laser pulse interactions with matter, and spectroscopic applications. *J Chem Phys* 83:5391–5399.
11. Kummrow A, Lau A (1996) Dynamics in condensed molecular systems studied by incoherent light. *Appl Phys B* 63:209–223.
12. Lau A, Pfeiffer M, Kummrow A (1996) Subpicosecond two-dimensional Raman spectroscopy applying broadband nanosecond laser radiation. *Chem Phys Lett* 263: 435–440.
13. Turner DB, Arpin PC, McClure SD, Ulness DJ, Scholes GD (2013) Coherent multidimensional optical spectra measured using incoherent light. *Nat Commun* 4:2298.
14. Tomita M, Masahiro M (1986) Ultrafast pump-probe measurement using intensity correlation of incoherent light. *J Opt Soc Am* 3:560–563.
15. Fassioli F, Dinshaw R, Arpin PC, Scholes GD (2013) Photosynthetic light harvesting: Excitons and coherence. *J R Soc Interface* 11:20130901.
16. Mukamel S, Rahav S (2010) Ultrafast nonlinear optical signals viewed from the molecule's perspective: Kramers-Heisenberg transition-amplitudes vs. susceptibilities. *Adv At Mol Opt Phys* 59:223–263.
17. Riek C, et al. (2015) Direct sampling of electric-field vacuum fluctuations. *Science* 350: 420–423.
18. Riek C, et al. (2017) Subcycle quantum electrodynamics. *Nature* 541:376–379.
19. Esposito M, et al. (2015) Photon number statistics uncover the fluctuations in non-equilibrium lattice dynamics. *Nat Commun* 6:10249, and erratum (2016) 7:10651.
20. Weninger C, et al. (2013) Stimulated electronic x-ray Raman scattering. *Phys Rev Lett* 111:233902.
21. Weiner AM (2000) Femtosecond pulse shaping using spatial light modulators. *Rev Sci Instrum* 71:1929–1960.
22. Rundquist A, Broman J, Underwood D, Blank D (2005) Polarization-dependent detection of impulsive stimulated Raman scattering in α-quartz. *J Mod Opt* 52: 2501–2510.
23. Dudovich N, Oron D, Silberberg Y (2002) Single-pulse coherently controlled nonlinear Raman spectroscopy and microscopy. *Nature* 418:512–514.
24. Kimberg V, Rohringer N (2016) Stochastic stimulated electronic x-ray Raman spectroscopy. *Struct Dyn* 3:034101.
25. Brüschweiler R, Zhang F (2004) Covariance nuclear magnetic resonance spectroscopy. *J Chem Phys* 120:5253–5260.